

Information Rates of Successive Interference Cancellation for Optical Fiber

Alex Jäger and Gerhard Kramer, *Fellow, IEEE*

Abstract—Successive interference cancellation (SIC) is used to approach the achievable information rates (AIRs) of joint detection and decoding for long-haul optical fiber links. The AIRs of memoryless ring constellations are compared to those of circularly symmetric complex Gaussian modulation for surrogate channel models with correlated phase noise. Simulations are performed for 1000 km of standard single-mode fiber with ideal Raman amplification. In this setup, 32 rings and 16 SIC-stages with Gaussian message-passing receivers achieve the AIR peaks of previous work. The computational complexity scales in proportion to the number of SIC-stages, where one stage has the complexity of separate detection and decoding.

Index Terms—Belief propagation, nonlinearity mitigation, optical fiber communication, phase noise, successive interference cancellation.

I. INTRODUCTION

Estimating the capacity of optical fiber is difficult because of the interactions of frequency-dependent attenuation, dispersion, and Kerr non-linearity [1]. A standard approach computes achievable information rates (AIRs) by simulating transmission and having the receiver process its signal via surrogate, or mismatched, models. The closer the surrogate model is to the actual model, as measured by an informational divergence, the higher the computed AIR. One, therefore, often has a trade-off between AIR and computational complexity.

For example, two useful surrogate models are a memoryless additive white Gaussian noise (AWGN) channel whose covariance and pseudo-covariance may depend on the channel input amplitude [1, Sec. X.C] and an AWGN channel with correlated phase noise with large memory [2], [3], [4]; see also [5], [6], [7], [8]. A memoryless model suggests practical receiver algorithms with a posteriori probability (APP) processing. The models with memory improve the AIR, but it is less clear how to build practical receivers. In particular, the receivers in [6], [7], [9], [8], [10] use particle filters to compute joint detection and decoding (JDD) rates, but it is not obvious how to convert such structures into practical systems.

Two classic methods to approach JDD performance combine separate detection and decoding (SDD) with either turbo processing or successive interference cancellation (SIC). The former approach was applied to Wiener phase noise channels [11], [12], [13] and fiber-optic systems [14], [15]. This method has the disadvantage of requiring receiver iterations and a

dedicated code design to maximize the rates. We instead use the SIC structure outlined in [1, Sec. XII] for which off-the-shelf codes and classic multi-level coded modulation approach capacity; see also [16], [17], [18] and recently [19], [20].

This paper is organized as follows. Sec. II introduces notation, the channel model, and the correlated phase and additive noise (CPAN) surrogate model of [9]. Sec. III and Sec. IV propose SIC receivers for circularly symmetric complex Gaussian (CSCG) modulation and ring constellations, respectively. The receivers use belief propagation and approximate message passing. For a sufficient number of SIC-stages, the receiver achieves, and even surpasses, the AIR for JDD predicted in [9]. Sec. V concludes the paper and suggests future work on implementations.

II. PRELIMINARIES

A. Notation

Random variables are written in uppercase, such as X , and their realizations in lowercase, such as x . Random vectors are written with bold letters, such as \mathbf{X} , and their realizations as \mathbf{x} . We write $a(x) \propto b(x)$ if there exists a constant c for which $a(x) = cb(x)$. A Gaussian X with mean μ and variance σ^2 has probability density function (pdf)

$$\mathcal{N}(x; \mu, \sigma^2) = \frac{1}{\sqrt{2\pi\sigma^2}} \exp\left(-\frac{1}{2} \frac{(x - \mu)^2}{\sigma^2}\right). \quad (1)$$

Similarly, a complex Gaussian X with mean μ , variance $\sigma^2 = \mathbb{E}[|X - \mu|^2]$ and pseudo-variance $p^2 = \mathbb{E}[(X - \mu)^2]$ has pdf

$$\mathcal{N}_{\mathbb{C}}(x; \mu, \sigma^2, p^2) = \frac{1}{\pi \sqrt{\sigma^2 \left(\sigma^2 - \frac{|p|^4}{\sigma^2}\right)}} \exp\left(-\frac{1}{2} [(x - \mu)^*, (x - \mu)] \begin{bmatrix} \sigma^2 & p^2 \\ (p^2)^* & \sigma^2 \end{bmatrix}^{-1} \begin{bmatrix} (x - \mu) \\ (x - \mu)^* \end{bmatrix}\right) \quad (2)$$

where $*$ denotes complex conjugation. A CSCG has $p^2 = 0$ and therefore the pdf

$$\mathcal{N}_{\mathbb{C}}(x; \mu, \sigma^2) = \frac{1}{\pi\sigma^2} \exp\left(-\frac{|x - \mu|^2}{\sigma^2}\right). \quad (3)$$

The function

$$m(x) = (x + \pi \bmod 2\pi) - \pi \quad (4)$$

maps x to the interval $[-\pi, \pi)$.

Alex Jäger and Gerhard Kramer are with the Chair of Communications Engineering, Department of Computer Engineering, School of Computation, Information and Technology, Technical University of Munich, 80333 Munich, Germany (e-mail: alex.jaeger@tum.de; gerhard.kramer@tum.de).

B. System Model

We use a standard model [1] for optical networks with reconfigurable optical add-drop multiplexers (ROADMs). Multiple wavelength-division multiplexing (WDM) channels co-propagate over a fiber span, and each receiver can access only its channel of interest (COI). Co-propagating channels disturb each other due to nonlinearities, such as cross-phase modulation (XPM) and four-wave mixing (FWM), and the worst-case scenario has different co-propagating signals over the entire length of the transmission link. The continuous-time baseband signal for n symbols and $2b$ interfering channels is

$$x(0, t) = \sum_{i=1}^n x_i g(t - iT) + \sum_{\substack{k=-b \\ k \neq 0}}^b \sum_{i=1}^n b_i^{(k)} g(t - iT) e^{j\omega_k t} \quad (5)$$

where the x_i and $b_i^{(k)}$ are realizations of mutually independent random variables with a common alphabet \mathcal{X} and variance σ_x^2 . All channels use root-raised cosine (RRC) pulse-shaping filters $g(\cdot)$ and symbol rate $1/T$. We assume $\|g\|^2/T = 1$, so the per-channel average transmit power is $P_{\text{tx}} = \sigma_x^2$. The central frequency of the k -th channel is $\omega_k/2\pi$ where $\omega_0 = 0$.

Signal propagation over an optical fiber using ideal distributed Raman amplification (IDRA) is described by the nonlinear Schrödinger equation (NLSE) [9]

$$\frac{\partial x(z, t)}{\partial z} = -j\frac{\beta_2}{2} \frac{\partial^2 x(z, t)}{\partial t^2} + j\gamma |x(z, t)|^2 x(z, t) + n(z, t) \quad (6)$$

where β_2 is the dispersion coefficient, γ the nonlinearity coefficient and $n(z, t)$ additive noise which is usually dominated by amplified spontaneous emission (ASE). The receiver accesses its COI via a bandpass filter with bandwidth $1/T$. It then performs sampling, single-channel digital backpropagation (DBP), matched filtering using RRC filters, downsampling to the symbol rate, and mean phase rotation compensation [9] to obtain the sequence $\{y_i\}$.

C. CPAN-Model

Surrogate models based on regular perturbation (RP) [21] simplify computation and analysis. We use the CPAN model from [9] that has a phase noise channel

$$Y_i = X_i e^{j\Theta_i} + N_i \quad (7)$$

where the transmit symbols $\{X_i\}$ are independent and identically distributed (i.i.d.). The additive noise process $\{N_i\}$ is white and CSCG with $p(n_i) = \mathcal{N}_{\mathbb{C}}(n_i; 0, \sigma_n^2)$, and the phase noise process $\{\Theta_i\}$ is a Markov chain with unit memory:

$$\Theta_i = \mu_\delta \Theta_{i-1} + \sigma_\delta \Delta_i \quad (8)$$

where $\{\Delta_i\}$ has i.i.d. real-valued, zero-mean, unit-variance, Gaussian Δ_i . We refer to [9, Equ. (56)] and [9, Equ. (50)] on how to choose μ_δ and σ_δ . We set the memory of the CPAN model to 1 because, without a whitening filter, the AIR hardly increases for larger memory. The additive and phase noise are independent of the transmit string

$$\mathbf{X} = [X_1, X_2, \dots, X_n]. \quad (9)$$

Unlike the Wiener phase noise model [6], the variance of Θ_i does not increase in i , and we have

$$\Theta_i \sim \mathcal{N}(0, \sigma_\theta^2) \quad \text{for all } i. \quad (10)$$

III. SIC FOR GAUSSIAN INPUTS

Consider CSCG inputs with $p(x_i) = \mathcal{N}_{\mathbb{C}}(x_i; 0, \sigma_x^2)$. SIC bridges the gap between AIRs for memoryless surrogate models [1] and AIRs for surrogate models with memory [9], [6]; see [19, Sec. IV]. For simplicity, we describe SIC with $S = 2$ stages and consider even n ; generalizing to any number of stages is straightforward.

The transmit vector \mathbf{x} of dimension n is divided into two vectors \mathbf{a} and \mathbf{b} of dimension $n/2$ in the manner

$$\mathbf{x} = [a_1, b_1, a_2, b_2, \dots, a_{n/2}, b_{n/2}]. \quad (11)$$

For the receive vector \mathbf{y} , a SIC decoder works in two stages:

- 1) Decode \mathbf{a} symbol-wise using the APPs $p(a_i|\mathbf{y})$ for all i .
- 2) Decode \mathbf{b} symbol-wise using the APPs $p(b_i|\mathbf{y}, \mathbf{a})$ for all i .

Note that the decoder receives APPs from the detector without any inter-symbol dependencies, i.e., $p(a_i|\mathbf{y})$ is independent of the a_k with $k \neq i$.

An AIR for the first stage with independent signaling is

$$I_1(\mathbf{A}; \mathbf{Y}) = \frac{1}{n/2} \sum_{i=1}^{n/2} h(A_i) - h(A_i|\mathbf{Y}) \leq I(\mathbf{A}; \mathbf{Y}) \quad (12)$$

where we used $h(A_i|\mathbf{Y}) \geq h(A_i|\mathbf{Y}, A_1, \dots, A_{i-1})$. For the second stage, an AIR is

$$I_2(\mathbf{B}; \mathbf{Y}|\mathbf{A}) = \frac{1}{n/2} \sum_{i=1}^{n/2} h(B_i) - h(B_i|\mathbf{Y}, \mathbf{A}) \leq I(\mathbf{B}; \mathbf{Y}|\mathbf{A}) \quad (13)$$

where we used $h(B_i|\mathbf{Y}, \mathbf{A}) \geq h(B_i|\mathbf{Y}, \mathbf{A}, B_1, \dots, B_{i-1})$. An AIR for SIC is the average of I_1 and I_2 :

$$I_{\text{sic}}(\mathbf{X}; \mathbf{Y}) = \frac{1}{2} (I_1(\mathbf{A}; \mathbf{Y}) + I_2(\mathbf{B}; \mathbf{Y}|\mathbf{A})) \leq I(\mathbf{X}; \mathbf{Y}). \quad (14)$$

A. Surrogate APP Based on the CPAN Model

The detector wishes to compute $p(a_i|\mathbf{y})$ and $p(b_i|\mathbf{y}, \mathbf{a})$. However, the true pdfs are unavailable, and we therefore use the surrogate probability

$$\begin{aligned} q(\mathbf{x}, \mathbf{y}, \boldsymbol{\theta}) &= p(\mathbf{x})p(\boldsymbol{\theta})q(\mathbf{y}|\mathbf{x}, \boldsymbol{\theta}) \\ &= \prod_{i=1}^n p(x_i)p(\theta_i|\theta_{i-1})q(y_i|x_i, \theta_i) \end{aligned} \quad (15)$$

with

$$p(x_i) = \mathcal{N}_{\mathbb{C}}(x_i; 0, \sigma_x^2) \quad (16)$$

$$p(\theta_i|\theta_{i-1}) = \mathcal{N}(\theta_i; \mu_\delta \theta_{i-1}, \sigma_\delta^2) \quad (17)$$

$$p(\theta_1) = \mathcal{N}(\theta_1; 0, \sigma_\theta^2) \quad (18)$$

$$q(y_i|x_i, \theta_i) = \mathcal{N}_{\mathbb{C}}(y_i; x_i e^{j\theta_i}, \sigma_n^2) \quad (19)$$

where we slightly abused notation for clarity.

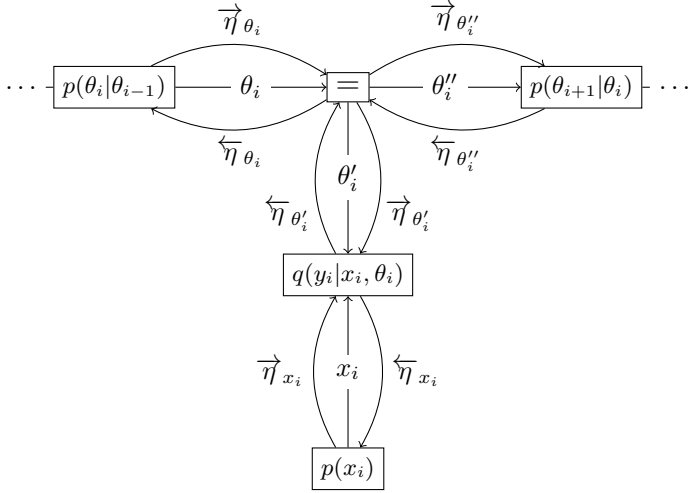


Fig. 1: Branch of the non-decoded stage.

Note that \mathbf{x} is a function of \mathbf{a} and \mathbf{b} . The surrogate model allows to approximate $p(a_i|\mathbf{y})$ and $p(b_i|\mathbf{y}, \mathbf{a})$ by

$$q(a_i|\mathbf{y}) = \frac{1}{c_1} \int_{\mathbb{R}^n} \int_{\mathcal{A} \setminus \{i\}} q(\mathbf{x}, \mathbf{y}, \boldsymbol{\theta}) d\mathbf{x} d\boldsymbol{\theta} \quad (20)$$

$$q(b_i|\mathbf{y}, \mathbf{a}) = \frac{1}{c_2} \int_{\mathbb{R}^n} \int_{\mathcal{B}_a \setminus \{i\}} q(\mathbf{x}, \mathbf{y}, \boldsymbol{\theta}) d\mathbf{x} d\boldsymbol{\theta} \quad (21)$$

where c_1 and c_2 are normalization factors and

$$\mathcal{A} \setminus \{i\} = \{\mathbf{x} \in \mathbb{C}^n : x_{2i-1} = a_i\} \quad (22)$$

$$\mathcal{B}_a \setminus \{i\} = \{\mathbf{x} \in \mathbb{C}^n : x_{2i} = b_i, [x_1, x_3, \dots, x_{n-1}] = \mathbf{a}\}. \quad (23)$$

We will marginalize $q(\mathbf{x}, \mathbf{y}, \boldsymbol{\theta})$ in both SIC-stages, where the marginalized variables depend on the stage.

B. Efficient Computation of the Marginal Distributions

The sum-product algorithm (SPA) computes the desired marginals; see [22], [23]. To illustrate the algorithm, we use factor graphs with directed edges carrying messages. The message of edge e in the arrow direction is denoted $\vec{\eta}_e(\cdot)$, and that in the opposite direction $\overleftarrow{\eta}_e(\cdot)$. In general, messages are densities, but for simplicity, we approximate most densities by real-valued Gaussians. In this case, $\vec{\mu}_e$ denotes the mean and $\vec{\sigma}_e^2$ the variance of $\vec{\eta}_e(\cdot)$, and likewise for $\overleftarrow{\eta}_e(\cdot)$.

1) *First Stage Detection*: Fig. 1 depicts the branches of the first SIC-stage.

Upward Path: The X_i are circularly symmetric, i.e., we have the relation $p(x_i) = p(x_i e^{j\theta})$ for all θ , which implies

$$\begin{aligned} \overleftarrow{\eta}_{\theta'_i}(\theta_i) &= \frac{1}{\overleftarrow{c}_{\theta'_i}} \int_{\mathbb{C}} p(x_i) q(y_i | x_i, \theta_i) dx_i \\ &= \frac{1}{\overleftarrow{c}_{\theta'_i}} \int_{\mathbb{C}} p(x'_i) q(y_i | x'_i) dx'_i = \text{const.} \end{aligned} \quad (24)$$

where $x'_i = x_i e^{j\theta_i}$. By $\frac{1}{\overleftarrow{c}_{\theta'_i}}$, and likewise for other messages, we denote a constant that normalizes to a valid pdf.

Rightward Path: Using $\vec{\eta}_{\theta_1}(\theta_1) = p(\theta_1)$, we obtain

$$\begin{aligned} \vec{\eta}_{\theta_2}(\theta_2) &= \frac{1}{\overleftarrow{c}_{\theta_2}} \int_{\mathbb{R}} \vec{\eta}_{\theta_1}(\theta_1) \overleftarrow{\eta}_{\theta'_1}(\theta_1) p(\theta_2 | \theta_1) d\theta_1 \\ &= \int_{\mathbb{R}} p(\theta_1) p(\theta_2 | \theta_1) d\theta_1 = p(\theta_2) \end{aligned} \quad (25)$$

and recursively $\vec{\eta}_{\theta_i}(\theta_i) = p(\theta_i)$ for all i .

Leftward Path: We similarly have

$$\begin{aligned} \overleftarrow{\eta}_{\theta''_{n-1}}(\theta_{n-1}) &= \frac{1}{\overleftarrow{c}_{\theta''_{n-1}}} \int_{\mathbb{R}} \overleftarrow{\eta}_{\theta'_n}(\theta_n) p(\theta_n | \theta_{n-1}) d\theta_n \\ &= \text{const.} \end{aligned} \quad (26)$$

and recursively $\overleftarrow{\eta}_{\theta'_i}(\theta_i)$ is constant in θ_i .

Downward Path: We have

$$\vec{\eta}_{\theta'_i}(\theta_i) = \frac{1}{\overleftarrow{c}_{\theta'_i}} \vec{\eta}_{\theta_i}(\theta_i) \overleftarrow{\eta}_{\theta''_i}(\theta_i) = p(\theta_i) \quad (27)$$

and

$$\begin{aligned} \overleftarrow{\eta}_{x_i}(x_i) &= \frac{1}{\overleftarrow{c}_{x_i}} \int_{\mathbb{R}} \vec{\eta}_{\theta'_i}(\theta_i) q(y_i | x_i, \theta_i) d\theta_i \\ &= \frac{1}{\overleftarrow{c}_{x_i}} \int_{\mathbb{R}} \mathcal{N}(\theta_i; 0, \sigma_\theta^2) \mathcal{N}(y_i; x_i e^{j\theta_i}, \sigma_n^2) d\theta_i. \end{aligned} \quad (28)$$

The surrogate APP $q(x_i|\mathbf{y})$ may now be calculated using

$$f_i(x_i) = \frac{1}{c_{f_i}} \vec{\eta}_{x_i}(x_i) \overleftarrow{\eta}_{x_i}(x_i) \quad (29)$$

where c_{f_i} normalizes f_i to a valid pdf.

We approximate f_i by a complex Gaussian density with mean $\mu_{f_i} = E_{f_i}[X]$, variance $\sigma_{f_i}^2 = E_{f_i}[|X - \mu_{f_i}|^2]$ and pseudo-variance $p_{f_i}^2 = E_{f_i}[(X - \mu_{f_i})^2]$. As derived in App. A, we thus have

$$q(x_i|\mathbf{y}) = \mathcal{N}_{\mathbb{C}}(x_i; \mu_{f_i}, \sigma_{f_i}^2, p_{f_i}^2) \quad (30)$$

with

$$\mu_{f_i} = y_i \frac{\sigma_x^2}{\sigma_y^2} \exp\left(-\frac{\sigma_\theta^2}{2}\right) \quad (31)$$

$$\sigma_{f_i}^2 = \frac{\sigma_x^2}{\sigma_y^2} \left(\sigma_n^2 + |y_i|^2 \frac{\sigma_x^2}{\sigma_y^2} \right) - |\mu_{f_i}|^2 \quad (32)$$

$$p_{f_i}^2 = y_i^2 \frac{\sigma_x^4}{\sigma_y^4} \exp(-2\sigma_\theta^2) - \mu_{f_i}^2 \quad (33)$$

where $\sigma_y^2 = \sigma_x^2 + \sigma_n^2$. At this point, we are interested only in $q(x_i|\mathbf{y})$ for odd i , as these are the symbols detected in the first SIC-stage.

2) *Second Stage Detection*: In the second stage, the symbols in \mathbf{x} with an odd index i , namely those described by \mathbf{a} , have been detected and decoded. Hence, branches of the form Fig. 1 and branches of the form Fig. 2 alternate. The former corresponds to the elements in \mathbf{b} or those with even index of \mathbf{x} , respectively, and the latter to those in \mathbf{a} or odd index of \mathbf{x} .

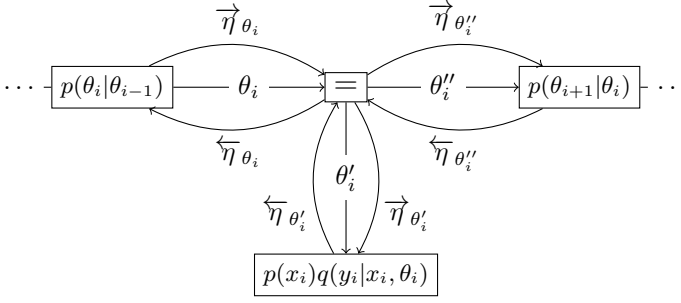


Fig. 2: Branch of the decoded stage.

Upward Path: For odd i , the message passed over θ'_i is

$$\begin{aligned} \overleftarrow{\eta}_{\theta'_i}(\theta_i) &= \frac{1}{\mathcal{C}_{\theta'_i}} p(x_i)q(y_i|x_i, \theta_i) \\ &= \frac{1}{\mathcal{C}_{\theta'_i}} \frac{p(x_i)}{\pi\sigma_n^2} \exp\left(-\frac{|y_i - x_i e^{j\theta_i}|^2}{\sigma_n^2}\right) \\ &\propto \exp\left(\frac{2|y_i||x_i|}{\sigma_n^2} \cos(\theta_i - (\angle y_i - \angle x_i))\right). \end{aligned} \quad (34)$$

This message consists of periodic repetitions of pulses, each similar to a Gaussian with mean $\angle y_i - \angle x_i + 2\pi k$ for $k \in \mathbb{N}$. As we show later on, messages on the left- and rightward paths, i.e., $\overrightarrow{\eta}_{\theta_i}$ and $\overleftarrow{\eta}_{\theta''_i}$, are Gaussians with near-zero mean and rapidly decaying tails. As products of these messages are passed on, we may focus on the period closest to zero by considering $m(\angle y_i - \angle x_i)$ which maps $\angle y_i - \angle x_i$ to the interval $[-\pi, \pi)$. Using the approximation $\cos(\gamma) \approx 1 - \gamma^2/2$, which is valid for small values of γ , we obtain

$$\overleftarrow{\eta}_{\theta'_i}(\theta_i) \approx \mathcal{N}\left(\theta_i; \overleftarrow{\mu}_{\theta'_i}, \overleftarrow{\sigma}_{\theta'_i}^2\right) \quad (35)$$

$$\overleftarrow{\mu}_{\theta'_i} = m(\angle y_i - \angle x_i) \quad (36)$$

$$\overleftarrow{\sigma}_{\theta'_i}^2 = \frac{\sigma_n^2}{2|y_i||x_i|}. \quad (37)$$

If i is even, as before, then $\overleftarrow{\eta}_{\theta'_i}(\theta_i)$ is constant in θ_i .

Rightward Path: We show that all messages in the rightward path are approximately Gaussian, that is

$$\overrightarrow{\eta}_{\theta_i}(\theta_i) \approx \mathcal{N}\left(\theta_i; \overrightarrow{\mu}_{\theta_i}, \overrightarrow{\sigma}_{\theta_i}^2\right) \quad (38)$$

$$\overrightarrow{\eta}_{\theta''_i}(\theta_i) \approx \mathcal{N}\left(\theta_i; \overrightarrow{\mu}_{\theta''_i}, \overrightarrow{\sigma}_{\theta''_i}^2\right). \quad (39)$$

If $\overrightarrow{\eta}_{\theta_i}$ is Gaussian, then $\overrightarrow{\eta}_{\theta''_i}$ is either a product of Gaussians or a product of a Gaussian and a constant, and hence Gaussian [24]. Explicitly, the parameters of $\overrightarrow{\eta}_{\theta''_i}$ depend on i as follows.

- If i is odd, then x_i was already decoded in the first stage and is a branch of the form shown in Fig. 2. Hence $\overrightarrow{\mu}_{\theta''_i}$ is a product of Gaussians and [24]

$$\overrightarrow{\mu}_{\theta''_i} = \frac{\overrightarrow{\mu}_{\theta_i} \overleftarrow{\sigma}_{\theta'_i}^2 + \overleftarrow{\mu}_{\theta'_i} \overrightarrow{\sigma}_{\theta_i}^2}{\overrightarrow{\sigma}_{\theta_i}^2 + \overleftarrow{\sigma}_{\theta'_i}^2} \quad (40)$$

$$\overrightarrow{\sigma}_{\theta''_i}^2 = \frac{\overrightarrow{\sigma}_{\theta_i}^2 \overleftarrow{\sigma}_{\theta'_i}^2}{\overrightarrow{\sigma}_{\theta_i}^2 + \overleftarrow{\sigma}_{\theta'_i}^2}. \quad (41)$$

- If i is even, then x_i was not decoded in the first stage and is a branch of the form shown in Fig. 1. Hence, $\overrightarrow{\eta}_{\theta''_i}$

is a product of a Gaussian and a constant, and therefore $\overrightarrow{\mu}_{\theta''_i} = \overrightarrow{\mu}_{\theta_i}$ and $\overrightarrow{\sigma}_{\theta''_i}^2 = \overrightarrow{\sigma}_{\theta_i}^2$.

If $\overrightarrow{\eta}_{\theta''_{i-1}}$ is Gaussian, then $\overrightarrow{\eta}_{\theta_i}$ is the marginalization over the product of a Gaussian and a conditional Gaussian. We have

$$\begin{aligned} \int_{\mathbb{R}} \mathcal{N}(\theta_{i-1}; \mu, \sigma^2) \mathcal{N}(\theta_i; \mu_\delta \theta_{i-1}, \sigma_\delta^2) d\theta_{i-1} \\ = \mathcal{N}(\theta_i; \mu_\delta \mu, \mu_\delta^2 \sigma^2 + \sigma_\delta^2) \end{aligned} \quad (42)$$

from which we obtain

$$\begin{aligned} \overrightarrow{\eta}_{\theta_i}(\theta_i) &= \int_{\mathbb{R}} \overrightarrow{\eta}_{\theta''_{i-1}}(\theta_{i-1}) p(\theta_i|\theta_{i-1}) d\theta_{i-1} \\ &\approx \mathcal{N}\left(\theta_i; \mu_\delta \overrightarrow{\mu}_{\theta''_{i-1}}, \mu_\delta^2 \overrightarrow{\sigma}_{\theta''_{i-1}}^2 + \sigma_\delta^2\right). \end{aligned} \quad (43)$$

With $\overrightarrow{\eta}_{\theta_1}(\theta_1) = p(\theta_1) = \mathcal{N}(\theta_1; 0, \sigma_\theta^2)$ for any stage, we arrive at (38)–(39) by induction.

Leftward Path: Denote by i' the largest index of all symbols decoded in earlier stages. In the second of two stages, $i' = n - 1$ if n is even and $i' = n$ else. All branches to the right of the i' -th branch are of the form shown in Fig. 1 and therefore $\overleftarrow{\eta}_{\theta''_{i'}}(\theta_{i'})$ is constant in $\theta_{i'}$. Therefore, we find that (note the different subscripts)

$$\overleftarrow{\eta}_{\theta_{i'}}(\theta_{i'}) = \overleftarrow{\eta}_{\theta''_{i'}}(\theta_{i'}) \quad (44)$$

is approximately Gaussian, see (35). This is also true for $i' = n$. If $\overleftarrow{\eta}_{\theta_{i+1}}$ is Gaussian in θ_{i+1} , then we update

$$\begin{aligned} \overleftarrow{\eta}_{\theta''_i}(\theta_i) &= \int_{\mathbb{R}} \overleftarrow{\eta}_{\theta_{i+1}}(\theta_{i+1}) p(\theta_{i+1}|\theta_i) d\theta_{i+1} \\ &\approx \mathcal{N}\left(\theta_i; \frac{\overleftarrow{\mu}_{\theta_{i+1}}}{\mu_\delta}, \frac{\overleftarrow{\sigma}_{\theta_{i+1}}^2 + \sigma_\delta^2}{\mu_\delta^2}\right). \end{aligned} \quad (45)$$

Similar to the rightward path, for $i \leq i'$, we have

$$\overleftarrow{\eta}_{\theta_i}(\theta_i) \approx \mathcal{N}\left(\theta_i; \overleftarrow{\mu}_{\theta_i}, \overleftarrow{\sigma}_{\theta_i}^2\right) \quad (46)$$

where the update rule depends on the index i .

- If i is odd, then

$$\overleftarrow{\mu}_{\theta_i} = \frac{\overleftarrow{\mu}_{\theta''_i} \overleftarrow{\sigma}_{\theta'_i}^2 + \overleftarrow{\mu}_{\theta'_i} \overleftarrow{\sigma}_{\theta''_i}^2}{\overleftarrow{\sigma}_{\theta'_i}^2 + \overleftarrow{\sigma}_{\theta''_i}^2} \quad (47)$$

$$\overleftarrow{\sigma}_{\theta_i}^2 = \frac{\overleftarrow{\sigma}_{\theta'_i}^2 \overleftarrow{\sigma}_{\theta''_i}^2}{\overleftarrow{\sigma}_{\theta'_i}^2 + \overleftarrow{\sigma}_{\theta''_i}^2}. \quad (48)$$

- If i is even, then $\overleftarrow{\mu}_{\theta_i} = \overleftarrow{\mu}_{\theta''_i}$ and $\overleftarrow{\sigma}_{\theta_i}^2 = \overleftarrow{\sigma}_{\theta''_i}^2$.

Downward Path: As both $\overrightarrow{\eta}_{\theta_i}(\theta_i)$ and $\overleftarrow{\eta}_{\theta''_i}(\theta_i)$ are Gaussian in θ_i , their product is also Gaussian. That is, we have

$$\begin{aligned} \overrightarrow{\eta}_{\theta''_i}(\theta_i) &= \frac{1}{\mathcal{C}_{\theta''_i}} \overrightarrow{\eta}_{\theta_i}(\theta_i) \overleftarrow{\eta}_{\theta''_i}(\theta_i) \\ &\approx \mathcal{N}\left(\theta_i; \overrightarrow{\mu}_{\theta''_i}, \overrightarrow{\sigma}_{\theta''_i}^2\right) \end{aligned} \quad (49)$$

with

$$\overrightarrow{\mu}_{\theta''_i} = \frac{\overrightarrow{\mu}_{\theta_i} \overleftarrow{\sigma}_{\theta'_i}^2 + \overleftarrow{\mu}_{\theta''_i} \overrightarrow{\sigma}_{\theta_i}^2}{\overrightarrow{\sigma}_{\theta_i}^2 + \overleftarrow{\sigma}_{\theta'_i}^2} \quad (50)$$

$$\overrightarrow{\sigma}_{\theta''_i}^2 = \frac{\overrightarrow{\sigma}_{\theta_i}^2 \overleftarrow{\sigma}_{\theta'_i}^2}{\overrightarrow{\sigma}_{\theta_i}^2 + \overleftarrow{\sigma}_{\theta'_i}^2}. \quad (51)$$

Similar to the first stage, for even i we approximate $q(x_i|\mathbf{y}, \mathbf{a})$ by a complex Gaussian. Simulations show that using CSCGs suffices, and the mean and variance are (see App. A)

$$\mu_{f_i} = y_i \frac{\sigma_x^2}{\sigma_y^2} \exp\left(-\frac{1}{2} \frac{\overrightarrow{\mu}_{\theta'_i}^2 - (\overrightarrow{\mu}_{\theta'_i} - j\overrightarrow{\sigma}_{\theta'_i}^2)^2}{\overrightarrow{\sigma}_{\theta'_i}^2}\right) \quad (52)$$

$$\sigma_{f_i}^2 = \frac{\sigma_x^2}{\sigma_y^2} \left(\sigma_n^2 + |y_i|^2 \frac{\sigma_x^2}{\sigma_y^2}\right) - |\mu_{f_i}|^2. \quad (53)$$

C. Extension to S SIC-Stages

An extension to S stages is straightforward. The first stage can be detected as described by (30)–(33). For stage $s > 1$, all x_i corresponding to stages $s' < s$ are assumed to be known. Also, the following means and variances should be calculated beforehand for appropriate indices i :

$$\overleftarrow{\mu}_{\theta'_i} = m(\angle_{y_i} - \angle_{x_i}), \quad \overleftarrow{\sigma}_{\theta'_i}^2 = \frac{\sigma_n^2}{2|y_i||x_i|}. \quad (54)$$

For Gaussian messages, we collect the mean and variance in one vector

$$\overrightarrow{\eta}_{\theta_i} = [\overrightarrow{\mu}_{\theta_i}, \overrightarrow{\sigma}_{\theta_i}^2] \quad (55)$$

and likewise for other messages. We also define the function

$$g(\eta_1, \eta_2) = \left[\frac{\mu_1 \sigma_2^2 + \mu_2 \sigma_1^2}{\sigma_1^2 + \sigma_2^2}, \frac{\sigma_1^2 \sigma_2^2}{\sigma_1^2 + \sigma_2^2} \right] \quad (56)$$

which describes the mean and variance of the product of Gaussians with parameters η_1 and η_2 .

Algorithm 1 shows the computations for stage s . The set \mathcal{I}_s has the symbol indices decoded in earlier stages, e.g., for $S = 2$ that is $\mathcal{I}_1 = \emptyset$ and $\mathcal{I}_2 = \{1, 3, \dots, n-1\}$. We have $\overrightarrow{\eta}_{\theta_1} = [0, \sigma_\theta^2]$. For $i' = n - S + (s - 1)$, which is the index of the last symbol in \mathbf{x} decoded prior to stage $s > 1$, we have

$$\overleftarrow{\eta}_{\theta_{i'}} = \left[m(\angle_{y_{i'}} - \angle_{x_{i'}}), \frac{\sigma_n^2}{2|y_{i'}||x_{i'}|} \right] \quad (57)$$

and (see (45))

$$\overleftarrow{\eta}_{\theta_{i'-1}} = \left[\frac{m(\angle_{y_{i'}} - \angle_{x_{i'}})}{\mu_\delta}, \frac{\frac{\sigma_n^2}{2|y_{i'}||x_{i'}|} + \sigma_\delta^2}{\mu_\delta^2} \right]. \quad (58)$$

Let $\mathbf{x}^{(s)}$ be the symbols decoded in stage s , i.e., for two stages $\mathbf{a} = \mathbf{x}^{(1)}$ and $\mathbf{b} = \mathbf{x}^{(2)}$. For $i \in \{s, s+S, s+2S, \dots\}$, we have

$$q(x_i|\mathbf{y}, \mathbf{x}^{(1)}, \dots, \mathbf{x}^{(s-1)}) = \mathcal{N}_{\mathbb{C}}(x_i; \mu_{f_i}, \sigma_{f_i}^2) \quad (59)$$

where μ_{f_i} and $\sigma_{f_i}^2$ can be calculated from the output of algorithm 1 and (52)–(53).

Note that our Gaussian approximate message passing algorithm uses messages that are vectors of dimension two with a mean and variance. Also, the calculations for the $\overleftarrow{\eta}_{\theta'_i}$, $\overrightarrow{\eta}_{\theta'_i}$, μ_{f_i} , and $\sigma_{f_i}^2$ can be parallelized.

Algorithm 1 SIC-Stage-Detector for Independent CSCG Inputs

Input: $\mathbf{y}, \mathbf{x}^{(1)}, \dots, \mathbf{x}^{(s-1)}, \mathcal{I}_s, s, S, n, i', \overrightarrow{\eta}_{\theta_1}, \overleftarrow{\eta}_{\theta_{i'-1}}, \overleftarrow{\eta}_{\theta_{i'}}$
for $i \in \mathcal{I}_s$

Output: $\overrightarrow{\eta}_{\theta'_i}$

▷ Rightward Path

for $i \leftarrow 1$ to $n - 1$ **do**

if $i \in \mathcal{I}_s$ **then**

$$\overrightarrow{\eta}_{\theta_{i'}} \leftarrow g(\overrightarrow{\eta}_{\theta_i}, \overleftarrow{\eta}_{\theta_{i'}})$$

else

$$\overrightarrow{\eta}_{\theta_{i'}} \leftarrow \overrightarrow{\eta}_{\theta_i}$$

end if

$$\overrightarrow{\eta}_{\theta_{i+1}} \leftarrow [\mu_\delta \overrightarrow{\mu}_{\theta_{i'}}, \mu_\delta^2 \overrightarrow{\sigma}_{\theta_{i'}}^2 + \sigma_\delta^2]$$

end for

▷ Leftward Path

for $i \leftarrow i' - 1$ to 2 **do**

if $i \in \mathcal{I}_s$ **then**

$$\overleftarrow{\eta}_{\theta_i} \leftarrow g(\overleftarrow{\eta}_{\theta_{i'}}, \overleftarrow{\eta}_{\theta_i})$$

else

$$\overleftarrow{\eta}_{\theta_i} \leftarrow \overleftarrow{\eta}_{\theta_{i'}}$$

end if

$$\overleftarrow{\eta}_{\theta_{i-1}} \leftarrow \left[\frac{\overleftarrow{\mu}_{\theta_i}}{\mu_\delta}, \frac{\overleftarrow{\sigma}_{\theta_i}^2 + \sigma_\delta^2}{\mu_\delta^2} \right]$$

end for

▷ Downward Path

for $l \leftarrow 0$ to $\lfloor n/S \rfloor - 1$ **do**

$i \leftarrow s + lS$

$$\overrightarrow{\eta}_{\theta'_i} \leftarrow g(\overrightarrow{\eta}_{\theta_i}, \overleftarrow{\eta}_{\theta_{i'}})$$

end for

D. Lower Bound on Mutual Information

We lower bound $I_1(\mathbf{A}; \mathbf{Y})$ by using

$$\begin{aligned} h_q(A_i|\mathbf{Y}) &= - \int p(\mathbf{y}) \int p(a_i|\mathbf{y}) \log q(a_i|\mathbf{y}) da_i d\mathbf{y} \\ &= h(A_i|\mathbf{Y}) + D(p(A_i|\mathbf{Y})||q(A_i|\mathbf{Y})) \\ &\geq h(A_i|\mathbf{Y}) \end{aligned} \quad (60)$$

where $D(\cdot||\cdot)$ is informational divergence that is non-negative. We thus have

$$I_{1,q}(\mathbf{A}; \mathbf{Y}) = \frac{1}{n/2} \sum_{i=1}^{n/2} h(A_i) - h_q(A_i|\mathbf{Y}) \leq I_1(\mathbf{A}; \mathbf{Y}). \quad (61)$$

Likewise, we have

$$I_{2,q}(\mathbf{B}; \mathbf{Y}|\mathbf{A}) := \frac{1}{n/2} \sum_{i=1}^{n/2} h(B_i) - h_q(B_i|\mathbf{Y}, \mathbf{A}) \leq I_2(\mathbf{B}; \mathbf{Y}|\mathbf{A}) \quad (62)$$

with

$$\begin{aligned} h_q(B_i|\mathbf{Y}, \mathbf{A}) &= - \int \int p(\mathbf{y}, \mathbf{a}) \int p(b_i|\mathbf{y}, \mathbf{a}) \\ &\quad \cdot \log q(b_i|\mathbf{y}, \mathbf{a}) db_i d\mathbf{y} d\mathbf{a}. \end{aligned} \quad (63)$$

As we use i.i.d. CSCG inputs with variance σ_x^2 , we have

$$h(A_i) = h(B_i) = \log(\pi e \sigma_x^2). \quad (64)$$

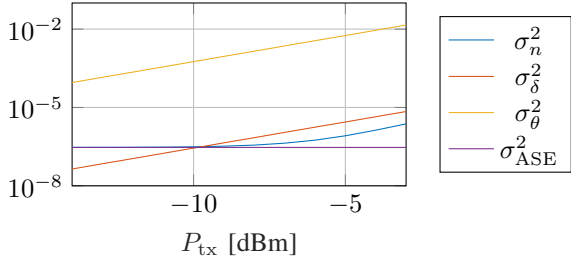


Fig. 3: Parameters considered in the CPAN model for the setup described by Table I and [9, Sec. VIII].

We approximate (60) and (63) by simulating transmission of N_{seq} sequences $\{\mathbf{x}_k\}$ and $\{\mathbf{y}_k\}$ and compute

$$h_q(A_i|\mathbf{Y}) \approx -\frac{1}{N_{\text{seq}}} \sum_{k=1}^{N_{\text{seq}}} \log q(a_{k,i}|\mathbf{y}_k) \quad (65)$$

$$h_q(B_i|\mathbf{Y}, \mathbf{A}) \approx -\frac{1}{N_{\text{seq}}} \sum_{k=1}^{N_{\text{seq}}} \log q(b_{k,i}|\mathbf{y}_k, \mathbf{a}_k). \quad (66)$$

E. Simulation Results

Table I lists the simulation parameters; see [9, Sec. VIII]. However, the receiver does not use a whitening filter and uses a unit-memory surrogate channel. We use 24 sequences of 8192 symbols each for training, e.g., to obtain μ_δ and σ_δ^2 , and 120 sequences of 8192 symbols each for testing, i.e., $N_{\text{seq}} = 120$.

We first investigate the AIRs of the CPAN channel with noise variances that mimic those of the nonlinear fiber-optic channel. Fig. 3 plots the variances σ_θ^2 , σ_δ^2 of the phase noise process, and the variance σ_n^2 of the AWGN. These variances increase with P_{tx} due to the nonlinear interference. In contrast, the variance σ_{ASE}^2 of the ASE is constant at approximately $2.95 \cdot 10^{-7}$.

Fig. 4a show the AIRs for the following benchmarking scenarios:

- ① a memoryless AWGN surrogate model,
- ② a memoryless surrogate model with i.i.d. Gaussian phase noise and independent AWGN,
- ③ a JDD-receiver based on particle filtering [6], [9], and
- ④ a genie-aided receiver with perfect knowledge of the phase noise, so the AIR is $I(\mathbf{X}; \mathbf{Y}|\Theta)$.

The solid black curve shows the AWGN channel capacity with ASE only, which upper bounds the CPAN channel capacity.

The inequality (14) shows that SIC cannot outperform JDD. SIC improves the memoryless receivers, and the memoryless phase noise receiver AIR is the same as the SIC AIR with $S = 1$. As Θ and \mathbf{X} are independent, we have $I(\mathbf{X}; \mathbf{Y}|\Theta) \geq I(\mathbf{X}; \mathbf{Y})$. Thus, the genie-aided receiver with perfect knowledge of the phase noise has larger AIRs than the JDD receiver.

Fig. 4a shows that SIC with 2 and 4 stages loses significant AIR compared to JDD. To maintain a rate loss of less than 1%, one needs at least 8 SIC-stages. The AIR of the SIC receiver with 64 stages is very close to the AIR of the genie-aided receiver with perfect knowledge of the phase noise process.

TABLE I: System Parameters

Parameter	Symbol	Value
Fiber Length	L	1000 km
Attenuation coefficient	α	0.2 dB km ⁻¹
Dispersion Coefficient	β_2	-21.7 ps ² km ⁻¹
Nonlinear coefficient	γ	1.27 W ⁻¹ km ⁻¹
Phonon occupancy factor	η	1
One-sided number of WDM channels	b	2

We infer that the proposed SIC receiver performs well for CPAN models. To further improve the rates for the nonlinear fiber-optic channel, one must improve the surrogate model, e.g., by considering correlations in the additive noise [6].

Studies of the dispersion-free nonlinear-fiber optic channel show that derived models with zero dispersion have AIRs that grow as $\frac{1}{2} \log(\text{SNR}) + \mathcal{O}(1)$ where $\text{SNR} \propto P_{\text{tx}}$; see [25], [26], [27], [28]. In contrast, the CPAN AIRs decrease with P_{tx} because the additive noise variance σ_n^2 increases with P_{tx} , see Fig. 3. Both the phase and amplitude of the signal experience distortions that increase with transmit power.

Fig. 4b shows the AIRs for the nonlinear fiber-optic channel with a receiver that uses the CPAN surrogate model. The solid curve again shows the capacity of the AWGN-channel distorted by ASE only, which upper bounds the capacity [29], [30]. We remark that the inequality in (14) does not hold for mismatched mutual information (MI), i.e., $1/2 (I_{1,q}(\mathbf{A}; \mathbf{Y}) + I_{2,q}(\mathbf{B}; \mathbf{Y}|\mathbf{A}))$ might exceed $I_q(\mathbf{X}; \mathbf{Y})$ based on JDD and particle filtering, as used in [9]. Second, the AIRs of JDD are slightly smaller than those in [9], which is mostly due to the lack of a whitening filter.

We again see that 8 SIC-stages provide AIRs similar to those of JDD. However, for 16 or more SIC-stages, the AIR of SIC exceeds that of JDD. We infer that the channel description of the SIC channel better approximates the true channel than JDD does. The 64-stage SIC-receiver gains approximately 0.52 bits per channel use (bpcu), or 6.4%, in rate over the memoryless AWGN receiver.

IV. SIC FOR RING CONSTELLATIONS

This section studies ring constellations. The transmit symbols have an independent amplitude R_i and phase Γ_i . The amplitude is sampled from a discrete distribution in $\mathcal{R} = \{\tilde{r}_1, \dots, \tilde{r}_{n_r}\}$, and the phase is sampled from a continuous distribution in $[-\pi, \pi)$. We use the distributions

$$P(\tilde{r}_i) = w_i, \quad p(\gamma_i) = \frac{1}{2\pi}, \quad \text{for } \gamma_i \in [-\pi, \pi). \quad (67)$$

Like CSCG inputs, ring constellations are circularly symmetric, and therefore we have (see (24))

$$\overleftarrow{\eta}_{\theta'_i}(\theta_i) = \frac{1}{c_{\theta'_i}} \int_{\mathcal{C}} p(x_i) q(y_i|x_i, \theta_i) dx_i = \text{const.} \quad (68)$$

Motivated by CSCG inputs, we use equidistant rings with $\tilde{r}_\ell = \ell \cdot \Delta r$ and probabilities w_ℓ that model a Rayleigh Distribution with variance σ_x^2 , i.e.,

$$w_\ell = \frac{\tilde{r}_\ell \exp\left(-\frac{\tilde{r}_\ell^2}{\sigma_x^2}\right)}{\sum_{m=1}^{n_r} \tilde{r}_m \exp\left(-\frac{\tilde{r}_m^2}{\sigma_x^2}\right)}. \quad (69)$$

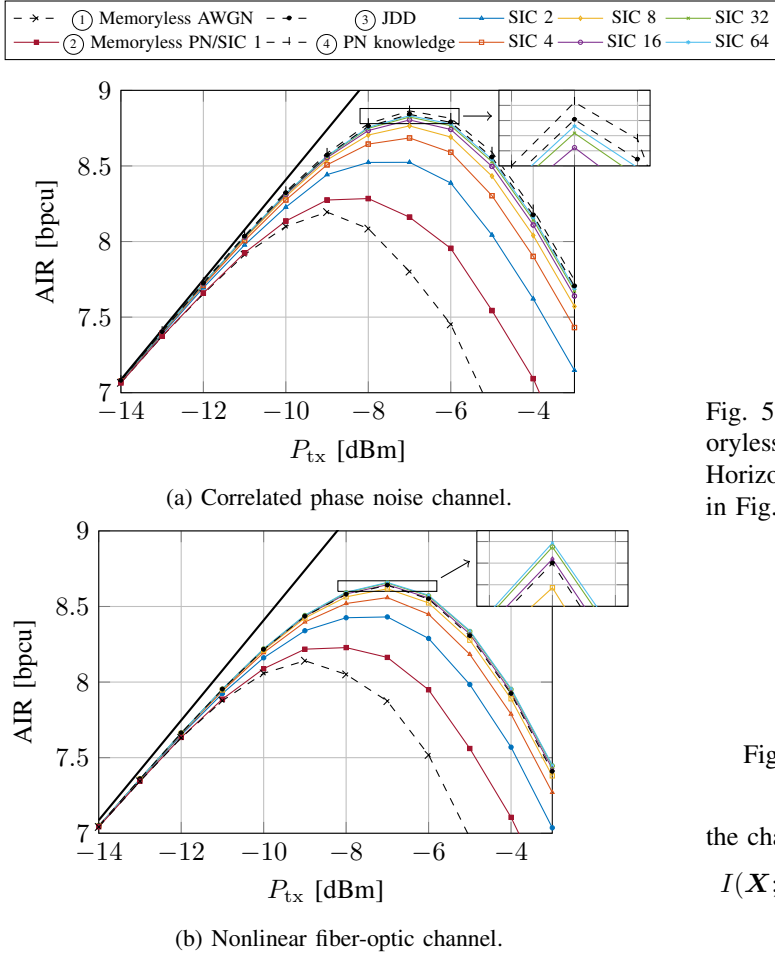


Fig. 4: AIR of various receivers for correlated phase noise and nonlinear fiber-optic channels. SIC with S stages is denoted SIC S . The solid black curves show a capacity upper bound.

We name this constellation unidistant Rayleigh ring (URR). The transmit power is

$$E[|X|^2] = \sigma_x^2 = \Delta r^2 \frac{\sum_{\ell=1}^{n_r} \ell^3 \exp\left(-\frac{\ell^2 \Delta r^2}{\sigma_x^2}\right)}{\sum_{\ell=1}^{n_r} \ell \exp\left(-\frac{\ell^2 \Delta r^2}{\sigma_x^2}\right)} \quad (70)$$

and we set $\sigma_x^2 = P_{tx}$. The Δr , which satisfies the power constraint, is found numerically.

URR constellations approximate a CSCG for large n_r . Fig. 5 shows the AIRs for memoryless AWGN channels with $\sigma_n^2 = 2.95 \cdot 10^{-7}$, which is approximately the ASE noise variance for the parameters in Table I. The horizontal line indicates the largest AIR of 2 SIC-stages in Fig. 4b, which is the peak value we attempt to reach. Observe that 32 rings are needed to prevent significant deviation from Gaussian inputs at the target AIR.

A. Mutual Information Estimation

Suppose \mathbf{X} has independent amplitudes \mathbf{R} and phases $\mathbf{\Gamma}$ that are transmitted through a channel $p_{\mathbf{Y}|\mathbf{X}}$; see Fig. 6. By

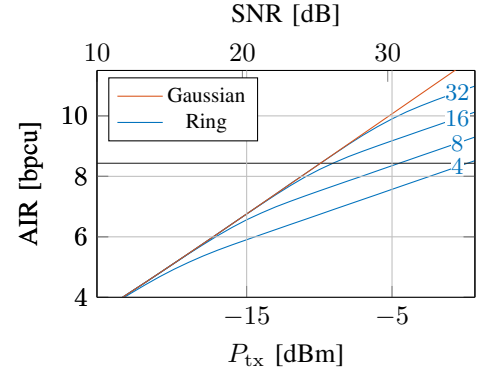


Fig. 5: AIR of Gaussian and ring constellations for memoryless AWGN channels with noise variance $2.95 \cdot 10^{-7}$. Horizontal line indicates the highest AIR for 2 SIC stages in Fig. 4b.

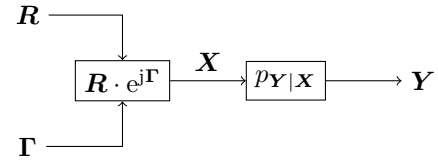


Fig. 6: Independently modulated phase and amplitude.

the chain rule of MI, we have

$$I(\mathbf{X}; \mathbf{Y}) + \underbrace{I(\mathbf{R}, \mathbf{\Gamma}; \mathbf{Y}|\mathbf{X})}_{=0} = I(\mathbf{R}, \mathbf{\Gamma}; \mathbf{Y}) + \underbrace{I(\mathbf{X}; \mathbf{Y}|\mathbf{R}, \mathbf{\Gamma})}_{=0} \quad (71)$$

and hence $I(\mathbf{X}; \mathbf{Y}) = I(\mathbf{R}; \mathbf{Y}) + I(\mathbf{\Gamma}; \mathbf{Y}|\mathbf{R})$. Consider (11) and define

$$a_i = r_{2i-1} \exp(j\alpha_i), \quad b_i = r_{2i} \exp(j\beta_i). \quad (72)$$

We divide only the phase noise vector into components related to \mathbf{a} and \mathbf{b} because, as we will show later, the absolute value can be detected and decoded in a memoryless fashion, hence no SIC receiver is needed.

AIRs for the absolute value and phase channels are

$$I_R(\mathbf{R}; \mathbf{Y}) = \frac{1}{n} \sum_{i=1}^n H(R_i) - H(R_i|\mathbf{Y})$$

$$I_1(\alpha; \mathbf{Y}|\mathbf{R}) = \frac{1}{n/2} \sum_{i=1}^{n/2} h(\alpha_i) - h(\alpha_i|\mathbf{Y}, \mathbf{R}) \quad (73)$$

$$I_2(\beta; \mathbf{Y}|\mathbf{R}, \alpha) = \frac{1}{n/2} \sum_{i=1}^{n/2} h(\beta_i) - h(\beta_i|\mathbf{Y}, \mathbf{R}, \alpha).$$

The following sum is an AIR for SIC:

$$I_{\text{sic}}(\mathbf{X}; \mathbf{Y}) = I_R(\mathbf{R}; \mathbf{Y}) + \frac{1}{2} \left(I_1(\alpha; \mathbf{Y}|\mathbf{R}) + I_2(\beta; \mathbf{Y}|\mathbf{R}, \alpha) \right) \leq I(\mathbf{X}; \mathbf{Y}). \quad (74)$$

Similar to (15), consider

$$q(\mathbf{r}, \alpha, \beta, \mathbf{y}, \theta) = q(\mathbf{r}, \gamma, \mathbf{y}, \theta)$$

$$= \prod_{i=1}^n P(r_i) p(\gamma_i) p(\theta_i|\theta_{i-1}) q(y_i|r_i, \gamma_i, \theta_i) \quad (75)$$

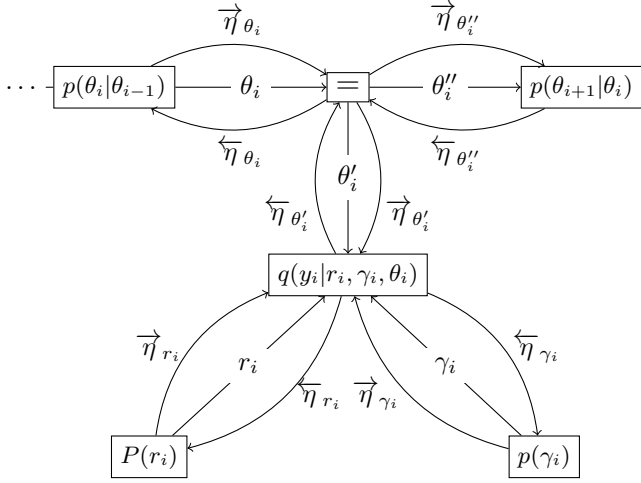


Fig. 7: Branch of the non-decoded stage with non-decoded absolute value.

where γ describes the angles of the entries of \mathbf{x} , and is thus a function of α and β . The vector \mathbf{x} is a function of \mathbf{r} and γ . As before, we discard dependencies for the sake of clarity. The receiver wishes to calculate

$$q(\mathbf{r}|\mathbf{y}) = \frac{1}{c_3} \int_{\mathbb{R}^n} \int_{\mathbf{\Pi}} \sum_{\mathbf{r} \in \mathcal{R} \setminus \{i\}} q(\mathbf{r}, \gamma, \mathbf{y}, \boldsymbol{\theta}) d\gamma d\boldsymbol{\theta} \quad (76)$$

$$q(\alpha_i|\mathbf{y}, \mathbf{r}) = \frac{1}{c_4} \int_{\mathbb{R}^n} \int_{\mathbf{\Pi} \setminus \{i\}} q(\mathbf{r}, \gamma, \mathbf{y}, \boldsymbol{\theta}) d\gamma d\boldsymbol{\theta} \quad (77)$$

$$q(\beta_i|\mathbf{y}, \mathbf{r}, \alpha) = \frac{1}{c_5} \int_{\mathbb{R}^n} \int_{\mathbf{\Pi} \setminus \{i\}} q(\mathbf{r}, \gamma, \mathbf{y}, \boldsymbol{\theta}) d\gamma d\boldsymbol{\theta} \quad (78)$$

where

$$\mathcal{R} \setminus \{i\} = \{\mathbf{r}' \in \mathcal{R}^n : r'_i = r_i\} \quad (79)$$

$$\mathbf{\Pi} = [-\pi, \pi]^n \quad (80)$$

$$\mathbf{\Pi} \setminus \{i\} = \{\gamma \in [-\pi, \pi]^n : \gamma_{2i-1} = \alpha_i\} \quad (81)$$

$$\mathbf{\Pi}_\alpha \setminus \{i\} = \{\gamma \in [-\pi, \pi]^n : \alpha(\gamma) = \alpha \wedge \gamma_{2i} = \beta_i\}. \quad (82)$$

with $\alpha(\gamma) = [\gamma_1, \gamma_3, \dots, \gamma_{n-1}]$. As before, we marginalize $q(\mathbf{r}, \gamma, \mathbf{y}, \boldsymbol{\theta})$, but the variables subject to marginalization depend on the SIC-stage.

B. Computing the Marginal Distributions

1) *Absolute Value Detection*: The graph used to detect the amplitudes \mathbf{r} has branches shown in Fig. 7. Using

$$\int_{-\pi}^{\pi} q(y_i|r_i, \gamma_i, \theta_i) d\gamma_i = \frac{2}{\sigma_n^2} \exp\left(-\frac{|y_i|^2 + r_i^2}{\sigma_n^2}\right) I_0\left(\frac{2|y_i|r_i}{\sigma_n^2}\right) \quad (83)$$

and $p(\gamma_i) = \frac{1}{2\pi}$, one can again show that

$$\begin{aligned} \overleftarrow{\eta}_{\theta'_i}(\theta_i) &= \frac{1}{c_{\theta'_i}} \sum_{r'_i \in \mathcal{R}} \int_{-\pi}^{\pi} p(\gamma_i) P(r_i) q(y_i|r_i, \gamma_i, \theta_i) d\gamma_i \\ &= \text{const.} \end{aligned} \quad (84)$$

As in (27), we obtain

$$\overrightarrow{\eta}_{\theta'_i}(\theta_i) = p(\theta_i) \quad (85)$$

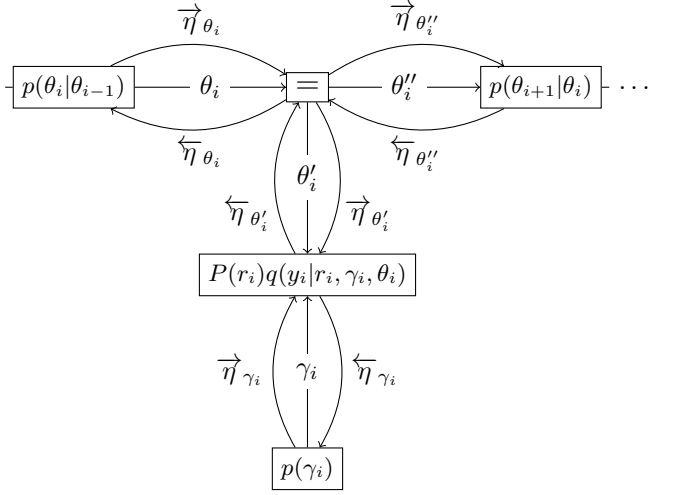


Fig. 8: Branch of the non-decoded stage with decoded absolute value.

and

$$\begin{aligned} \overleftarrow{\eta}_{r_i}(r_i) &= \frac{1}{c_{r_i}} \int_{\mathbb{R}} \overrightarrow{\eta}_{\theta'_i}(\theta_i) \int_{-\pi}^{\pi} p(\gamma_i) q(y_i|r_i, \gamma_i, \theta_i) d\gamma_i d\theta_i \\ &\propto \exp\left(-\frac{r_i^2}{\sigma_n^2}\right) I_0\left(\frac{2|y_i|r_i}{\sigma_n^2}\right). \end{aligned} \quad (86)$$

With this, upon receiving y_i one can compute

$$q(r_i|\mathbf{y}) = \frac{P(r_i) \overleftarrow{\eta}_{r_i}(r_i)}{\sum_{\tilde{r} \in \mathcal{R}} P(\tilde{r}) \overleftarrow{\eta}_{r_i}(\tilde{r})}. \quad (87)$$

Note that the computations for different i may run in parallel.

We now investigate SIC with two stages for absolute value detection. In the second stage, branches of the type shown in Fig. 7 and Fig. 8 alternate. For odd i , we have branches of the form shown in Fig. 8 and

$$\begin{aligned} \overleftarrow{\eta}_{\theta'_i}(\theta_i) &= \frac{1}{c_{\theta'_i}} \int_{-\pi}^{\pi} p(\gamma_i) q(y_i|r_i, \gamma_i, \theta_i) d\gamma_i \\ &= \text{const.} \end{aligned} \quad (88)$$

where we used (83). Following the same steps as before, we recover (87). Therefore, the receiver does not use the entries of \mathbf{r} decoded in the first stage. We can hence use (87) to detect all elements in \mathbf{r} and achieve no gain using SIC.

2) *Phase Detection, First Stage*: The graph is a concatenation of branches of the form shown in Fig. 8. Using (83), we again have $\overleftarrow{\eta}_{\theta'_i}(\theta_i) = \text{const.}$, and $\overrightarrow{\eta}_{\theta'_i}(\theta_i) = p(\theta_i)$. Similar to (34), we obtain

$$\begin{aligned} q(y_i|r_i, \gamma_i, \theta_i) &\approx \\ &\frac{1}{\sqrt{|y_i|r_i}} \mathcal{N}\left(|y_i|; r_i, \frac{\sigma_n^2}{2}\right) \mathcal{N}\left(\theta_i; m(\angle y_i - \gamma_i), \frac{\sigma_n^2}{2|y_i|r_i}\right). \end{aligned} \quad (89)$$

Using $\overrightarrow{\eta}_{\theta'_i}(\theta_i) = \mathcal{N}(\theta_i; 0, \sigma_\theta^2)$, we thus have

$$\begin{aligned} q(\gamma_i|\mathbf{y}, \mathbf{r}) &= \frac{1}{c_6} \overrightarrow{\eta}_{\gamma_i}(\gamma_i) \int_{\mathbb{R}} \overrightarrow{\eta}_{\theta'_i}(\theta_i) q(y_i|r_i, \gamma_i, \theta_i) d\theta_i \\ &\approx \mathcal{N}\left(m(\angle y_i - \gamma_i); 0, \sigma_\theta^2 + \frac{\sigma_n^2}{2|y_i|r_i}\right). \end{aligned} \quad (90)$$

The scaling constant ensures (90) has unit integral over the support of γ_i . However, as the tails decay rapidly, this constant is larger than, but very close to 1 and may be omitted.

3) *Phase Detection, Second Stage*: Branches of the form shown in Fig. 2 for odd i and Fig. 8 for even i alternate. In the former case, we use the approximation (35), while in the latter case $\overleftarrow{\eta}_{\theta'_i}(\theta_i)$ is constant in θ_i . With the same steps as before, we obtain

$$\overleftarrow{\eta}_{\theta'_i}(\theta_i) \approx \mathcal{N}\left(\theta_i; \overleftarrow{\mu}_{\theta'_i}, \overleftarrow{\sigma}_{\theta'_i}^2\right) \quad (91)$$

where (50) and (51) give the expressions for $\overleftarrow{\mu}_{\theta'_i}$ and $\overleftarrow{\sigma}_{\theta'_i}^2$. Similar to (90), we now have

$$q(\gamma_i|\mathbf{y}, \mathbf{r}, \boldsymbol{\alpha}) = \mathcal{N}\left(m(\angle y_i - \gamma_i - \overleftarrow{\mu}_{\theta'_i}); 0, \overleftarrow{\sigma}_{\theta'_i}^2 + \frac{\sigma_n^2}{2|y_i|r_i}\right) \quad (92)$$

where we omitted the normalization, as discussed above.

C. Extension to S SIC-Stages

Extending the algorithm to S stages is straightforward. We first decode \mathbf{r} using (87) and the first stage of γ using (90). For the s -th stage, we reuse algorithm 1 to obtain $\overleftarrow{\eta}_{\theta'_i} = \left[\overleftarrow{\mu}_{\theta'_i}, \overleftarrow{\sigma}_{\theta'_i}^2\right]$ and calculate $q(\gamma_i|\mathbf{y}, \mathbf{r}, \gamma^{(1)}, \dots, \gamma^{(s-1)})$ for $i \in \{s, s+S, s+2S, \dots\}$, as indicated by (92).

D. Lower Bound on Mutual Information

Using the same approach as in Sec. III-D, define

$$I_{R,q}(\mathbf{R}; \mathbf{Y}) = \frac{1}{n} \sum_{i=1}^n H(R_i) - H_q(R_i|Y_i) \quad (93)$$

$$\leq I_R(\mathbf{R}; \mathbf{Y})$$

$$I_{1,q}(\boldsymbol{\alpha}; \mathbf{Y}|\mathbf{R}) = \frac{1}{n/2} \sum_{i=1}^{n/2} h(\alpha_i) - h_q(\alpha_i|\mathbf{Y}, \mathbf{R}) \quad (94)$$

$$\leq I_1(\boldsymbol{\alpha}; \mathbf{Y}|\mathbf{R})$$

$$I_{2,q}(\boldsymbol{\beta}; \mathbf{Y}|\mathbf{R}, \boldsymbol{\alpha}) = \frac{1}{n/2} \sum_{i=1}^{n/2} h(\beta_i) - h_q(\beta_i|\mathbf{Y}, \mathbf{R}, \boldsymbol{\alpha}) \quad (95)$$

$$\leq I_2(\boldsymbol{\beta}; \mathbf{Y}|\mathbf{R}, \boldsymbol{\alpha}).$$

Note that

$$H(R_i) = - \sum_{\ell=1}^{n_r} w_\ell \log w_\ell, \quad h(\alpha_i) = h(\beta_i) = \log 2\pi \quad (96)$$

for all i . The surrogate channel (differential) conditional entropies can be approximated by simulation as in Sec. III-D.

E. Simulation Results

Fig. 9 shows the AIRs for 2 SIC-stages. The AIRs of CSCG modulation are plotted in dashed black for reference. As expected from Fig. 5, the AIR increases with the number of rings and saturates at 32 rings. Fig. 10 shows the rates as a function of the number of SIC-stages for 32 rings. This is similar to the results for CSCG modulation in Fig. 4.

The phase noise variance depends on the amplitude statistics. For example, M -PSK or ring constellations with one ring

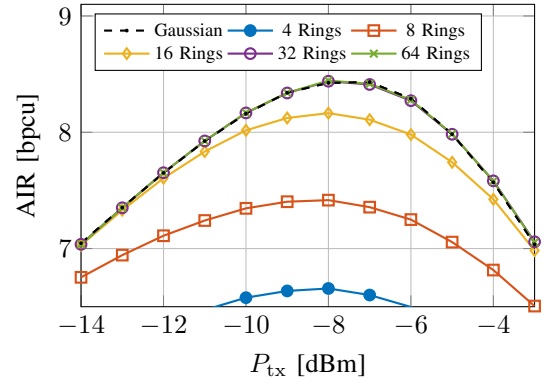


Fig. 9: AIR for 2 SIC-stages for Gaussian modulation and ring constellations.

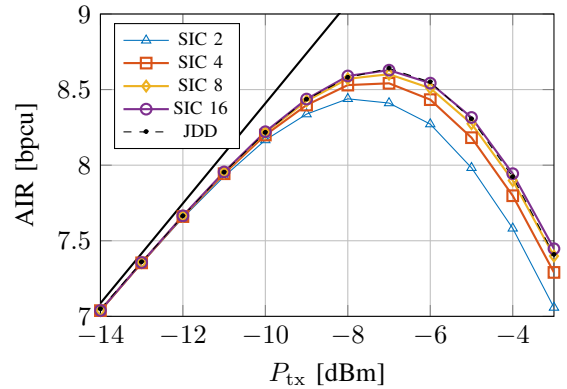


Fig. 10: AIR of ring constellations with 32 rings for different numbers of SIC-stages and the JDD receiver with Gaussian inputs for reference. The solid black curve shows a capacity upper bound.

cause little phase noise, whereas Gaussian modulation causes significant phase noise [5]. Therefore, we have a tradeoff: increasing the number of rings increases the amplitude channel's rate and the phase noise variance. The left plot in Fig. 11 shows that for two SIC-stages, the AIR of the phase channel decreases with an increasing number of rings. The right side shows that the AIR of the amplitude channel increases by a larger amount, and hence the overall AIR increases for an increasing number of rings.

V. CONCLUSION & OUTLOOK

We studied SIC-receivers to compensate for nonlinearity in optical fiber. The receiver used the CPAN model as a surrogate channel, and we simplified the SPA by using Gaussian messages. We proposed receiver algorithms for CSCG modulation and ring constellations that provide AIRs comparable to those of JDD receivers [9] for 16 or more SIC-stages. The ring constellations perform as well as CSCG modulation for 32 or more rings. For future work, we plan to study discrete constellations and multi-level coding with off-the-shelf codes, as well as dual-polarization and space-division multiplexing. Another interesting direction is to discard single-channel back-

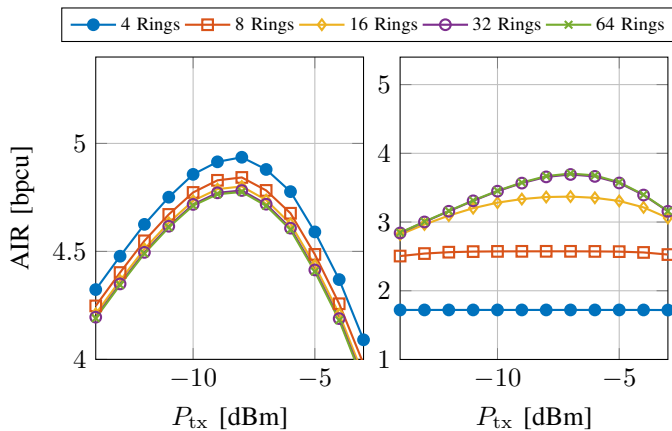


Fig. 11: AIR of phase (left) and amplitude (right) channel for two SIC-stages and ring constellations.

propagation and use the proposed receiver to compensate for self-phase modulation.

ACKNOWLEDGMENT

The authors wish to thank Daniel Plabst for inspiring discussions.

The authors acknowledge the financial support by the Federal Ministry of Education and Research of Germany in the programme of ‘‘Souver an. Digital. Vernetzt.’’. Joint project 6G-life, project identification number: 16KISK002.

APPENDIX A MOMENTS OF f

For CSCG inputs, let

$$f(x) = \frac{1}{c_f} p(x) \int_{\mathbb{R}} \vec{\eta}_{\theta'}(\theta) q(y|x, \theta) d\theta \quad (97)$$

and

$$\begin{aligned} c_f &= \int_{\mathbb{R}} \vec{\eta}_{\theta'}(\theta) \int_{\mathbb{C}} p(x) q(y|x, \theta) dx d\theta \\ &= q(y) \end{aligned} \quad (98)$$

with $q(y) = \mathcal{N}_{\mathbb{C}}(y; 0, \sigma_y^2)$. Using

$$g(x) = \begin{cases} x, & \text{for } E_f[X] \\ |x|^2, & \text{for } E_f[|X|^2] \\ x^2, & \text{for } E_f[X^2] \end{cases} \quad (99)$$

the second-order moments can be calculated with

$$\begin{aligned} &\int_{\mathbb{C}} g(x) f(x) dx \\ &= \underbrace{\int_{\mathbb{R}} \vec{\eta}_{\theta'}(\theta) e^{-kj\theta} d\theta}_{=:a} \int_{\mathbb{C}} g(\tilde{x}) \underbrace{\frac{p(\tilde{x})q(y|\tilde{x}, 0)}{q(y)}}_{=:b(\tilde{x})} d\tilde{x} \end{aligned} \quad (100)$$

where $\tilde{x} = xe^{j\theta}$ and $k = 1$ for $E_f[X]$, $k = 0$ for $E_f[|X|^2]$, and $k = 2$ for $E_f[X^2]$.

Using $\vec{\eta}_{\theta'}(\theta) = \mathcal{N}(\theta; \vec{\mu}_{\theta'}, \vec{\sigma}_{\theta'}^2)$ and completing the squares gives

$$a = \exp\left(-\frac{1}{2} \frac{\vec{\mu}_{\theta'}^2 - (\vec{\mu}_{\theta'} - k\vec{j}\vec{\sigma}_{\theta'}^2)^2}{\vec{\sigma}_{\theta'}^2}\right). \quad (101)$$

Also, $b(\tilde{x})$ is a CSCG

$$b(\tilde{x}) = \mathcal{N}_{\mathbb{C}}\left(\tilde{x}; y \frac{\sigma_x^2}{\sigma_y^2}, \frac{\sigma_x^2 \sigma_n^2}{\sigma_y^2}\right) \quad (102)$$

and therefore

$$\int_{\mathbb{C}} g(\tilde{x}) b(\tilde{x}) d\tilde{x} = \begin{cases} y \frac{\sigma_x^2}{\sigma_y^2}, & \text{for } g(\tilde{x}) = \tilde{x} \\ \frac{\sigma_x^2}{\sigma_y^2} \left(\sigma_n^2 + |y|^2 \frac{\sigma_x^2}{\sigma_y^2}\right), & \text{for } g(\tilde{x}) = |\tilde{x}|^2. \\ y^2 \frac{\sigma_x^4}{\sigma_y^4}, & \text{for } g(\tilde{x}) = \tilde{x}^2. \end{cases} \quad (103)$$

The moments of f follow directly:

$$\mu_f = y \frac{\sigma_x^2}{\sigma_y^2} \exp\left(-\frac{1}{2} \frac{\vec{\mu}_{\theta'}^2 - (\vec{\mu}_{\theta'} - \vec{j}\vec{\sigma}_{\theta'}^2)^2}{\vec{\sigma}_{\theta'}^2}\right) \quad (104)$$

$$\sigma_f^2 = \frac{\sigma_x^2}{\sigma_y^2} \left(\sigma_n^2 + |y|^2 \frac{\sigma_x^2}{\sigma_y^2}\right) - |\mu_f|^2 \quad (105)$$

$$p_f^2 = y^2 \frac{\sigma_x^4}{\sigma_y^4} \exp\left(-\frac{1}{2} \frac{\vec{\mu}_{\theta'}^2 - (\vec{\mu}_{\theta'} - 2\vec{j}\vec{\sigma}_{\theta'}^2)^2}{\vec{\sigma}_{\theta'}^2}\right) - \mu_f^2. \quad (106)$$

REFERENCES

- [1] R.-J. Essiambre, G. Kramer, P. J. Winzer, G. J. Foschini, and B. Goebel, ‘‘Capacity Limits of Optical Fiber Networks,’’ *J. Lightw. Technol.*, vol. 28, no. 4, pp. 662–701, 2010.
- [2] A. Mecozzi and R. Essiambre, ‘‘Nonlinear Shannon limit in pseudolinear coherent systems,’’ *J. Lightw. Technol.*, vol. 30, no. 12, pp. 2011–2024, June 2012.
- [3] R. Dar, M. Feder, A. Mecozzi, and M. Shtaif, ‘‘Properties of nonlinear noise in long, dispersion-uncompensated fiber links,’’ *Opt. Express*, vol. 21, no. 22, pp. 25 685–25 699, Nov 2013.
- [4] R. Dar, M. Shtaif, and M. Feder, ‘‘New bounds on the capacity of the nonlinear fiber-optic channel,’’ *Opt. Lett.*, vol. 39, no. 2, pp. 398–401, Jan 2014.
- [5] R. Dar, M. Feder, A. Mecozzi, and M. Shtaif, ‘‘Pulse Collision Picture of Inter-Channel Nonlinear Interference in Fiber-Optic Communications,’’ *J. Lightw. Technol.*, vol. 34, no. 2, pp. 593–607, 2016.
- [6] M. Secondini, E. Agrell, E. Forestieri, D. Marsella, and M. R. Camara, ‘‘Nonlinearity Mitigation in WDM Systems: Models, Strategies, and Achievable Rates,’’ *J. Lightw. Technol.*, vol. 37, no. 10, pp. 2270–2283, 2019.
- [7] M. Secondini, S. Civielli, E. Forestieri, and L. Z. Khan, ‘‘New lower bounds on the capacity of optical fiber channels via optimized shaping and detection,’’ *J. Lightw. Technol.*, vol. 40, no. 10, pp. 3197–3209, 2022.
- [8] F. J. Garc a-G omez and G. Kramer, ‘‘Mismatched models to lower bound the capacity of dual-polarization optical fiber channels,’’ *J. Lightw. Technol.*, vol. 39, no. 11, pp. 3390–3399, 2021.
- [9] —, ‘‘Mismatched Models to Lower Bound the Capacity of Optical Fiber Channels,’’ *J. Lightw. Technol.*, vol. 38, no. 24, pp. 6779–6787, 2020.
- [10] J. Dauwels and H.-A. Loeliger, ‘‘Computation of information rates by particle methods,’’ *IEEE Trans. Inf. Theory*, vol. 54, no. 1, pp. 406–409, 2008.
- [11] —, ‘‘Phase estimation by message passing,’’ in *IEEE Int. Conf. Commun.*, vol. 1, 2004, pp. 523–527 Vol.1.
- [12] G. Colavolpe, A. Barbieri, and G. Caire, ‘‘Algorithms for Iterative Decoding in the Presence of Strong Phase Noise,’’ *IEEE J. Selected Areas Commun.*, vol. 23, no. 9, pp. 1748–1757, 2005.
- [13] S. Shayovitz and D. Raphaeli, ‘‘Message passing algorithms for phase noise tracking using Tikhonov mixtures,’’ *IEEE Trans. Commun.*, vol. 64, no. 1, pp. 387–401, 2016.
- [14] M. P. Yankov, T. Fehenberger, L. Barletta, and N. Hanik, ‘‘Low-complexity tracking of laser and nonlinear phase noise in WDM optical fiber systems,’’ *J. Lightw. Technol.*, vol. 33, no. 23, pp. 4975–4984, 2015.
- [15] A. F. Alfredsson, E. Agrell, and H. Wymeersch, ‘‘Iterative detection and phase-noise compensation for coded multichannel optical transmission,’’ *IEEE Trans. Commun.*, vol. 67, no. 8, pp. 5532–5543, 2019.

- [16] U. Wachsmann, R. F. Fischer, and J. B. Huber, "Multilevel codes: Theoretical concepts and practical design rules," *IEEE Trans. Inf. Theory*, vol. 45, no. 5, pp. 1361–1391, 1999.
- [17] H. Pfister, J. Soriaga, and P. Siegel, "On the achievable information rates of finite state ISI channels," in *IEEE Global Telecommun. Conf.*, vol. 5, 2001, pp. 2992–2996 vol.5.
- [18] J. B. Soriaga, H. D. Pfister, and P. H. Siegel, "Determining and approaching achievable rates of binary intersymbol interference channels using multistage decoding," *IEEE Trans. Inf. Theory*, vol. 53, no. 4, pp. 1416–1429, 2007.
- [19] T. Prinz, D. Plabst, T. Wiegart, S. Calabrò, N. Hanik, and G. Kramer, "Successive Interference Cancellation for Bandlimited Channels with Direct Detection," *IEEE Trans. Commun.*, vol. 72, no. 3, pp. 1330–1340, 2024.
- [20] D. Plabst, T. Prinz, F. Diedolo, T. Wiegart, G. Böcherer, N. Hanik, and G. Kramer, "Neural network equalizers and successive interference cancellation for bandlimited channels with a nonlinearity," *IEEE Trans. Commun.*, submitted, 2024. [Online]. Available: <https://arxiv.org/abs/2401.09217>
- [21] A. Mecozzi and R.-J. Essiambre, "Nonlinear Shannon limit in pseudo-linear coherent systems," *J. Lightw. Technol.*, vol. 30, no. 12, pp. 2011–2024, 2012.
- [22] F. Kschischang, B. Frey, and H.-A. Loeliger, "Factor graphs and the sum-product algorithm," *IEEE Trans. Inf. Theory*, vol. 47, no. 2, pp. 498–519, 2001.
- [23] H.-A. Loeliger, "An introduction to factor graphs," *IEEE Signal Proc. Mag.*, vol. 21, no. 1, pp. 28–41, 2004.
- [24] P. Bromiley, "Products and convolutions of Gaussian probability density functions," University of Manchester, Tech. Rep., 2014.
- [25] K. S. Turitsyn, S. A. Derevyanko, I. V. Yurkevich, and S. K. Turitsyn, "Information capacity of optical fiber channels with zero average dispersion," *Phys. Rev. Lett.*, vol. 91, p. 203901, 2003.
- [26] M. I. Yousefi and F. R. Kschischang, "On the per-sample capacity of nondispersive optical fibers," *IEEE Trans. Inf. Theory*, vol. 57, no. 11, pp. 7522–7541, 2011.
- [27] G. Kramer, "Autocorrelation function for dispersion-free fiber channels with distributed amplification," *IEEE Trans. Inf. Theory*, vol. 64, no. 7, pp. 5131–5155, 2018.
- [28] C. Häger and E. Agrell, "Data-driven estimation of capacity upper bounds," *IEEE Commun. Lett.*, vol. 26, no. 12, pp. 2939–2943, 2022.
- [29] G. Kramer, M. I. Yousefi, and F. R. Kschischang, "Upper bound on the capacity of a cascade of nonlinear and noisy channels," in *IEEE Inf. Theory Workshop*, 2015, pp. 1–4.
- [30] M. I. Yousefi, G. Kramer, and F. R. Kschischang, "Upper bound on the capacity of the nonlinear Schrödinger channel," in *IEEE Can. Workshop Inf. Theory*, 2015, pp. 22–26.